Supplementary information

Kosmotropic-Effect-Driven Biphasic Aqueous Electrolyte towards Durable Zinc-Ion Batteries

Lianwen He, [a] *Long Su,* [a] *Xinming Xu,* [b] *Chongjiong Zheng,* [a] *Hui Gu,* [a] *Fusheng Pan,**[a] *Xinpei Gao,**[a] *and Fei Lu* *[a]

[a] School of Chemistry and Chemical Engineering, Hainan University, Haikou, Hainan, 570228, P. R. China

E-mail: fspan@hainanu.edu.cn; xpgao@hainanu.edu.cn; lufei@hainanu.edu.cn

[b] Key Laboratory of Colloid and Interface Chemistry, Shandong University, Jinan, Shandong, 250100, P. R. China

*Corresponding authors. Email: fspan@hainanu.edu.cn; xpgao@hainanu.edu.cn; lufei@hainanu.edu.cn

1. Experimental Section

1.1. Materials

All reagents were purchased and used directly without purification. 1-Propanol (AR), ethanol (AR), methanol (AR), zinc sulfate heptahydrate ($ZnSO_4 \cdot 7H_2O$, AR), zinc bis(trifluoromethylsulfonyl)imide ($Zn(TFSI)_2$, 98%), and N-methyl-2-pyrrolidine (NMP, ≥ 99.5%) were purchased from Sigma-Aldrich. Polyaniline (PANI, 98%) was acquired from Shanghai Macklin Biochemical Co. Ltd. Polyvinylidene fluoride (PVDF), Zn-foils, Cu-foils, PP membranes, Glass fibers, and Ketjen black (ECP-600JD) were provided by Guangdong Canrd New Energy Technology Co. Ltd.

1.2. Preparation of biphasic liquid electrolyte

To synthesize the biphasic liquid electrolytes, water and 1-propanol were initially mixed with a certain volume ratio of 1:1. Then, 0.87 g of $ZnSO_4 \cdot 7H_2O$ and 0.26 g of $Zn(TFSI)_2$ were dissolved in the above mixtures. Due to density differences, the solution was automatically separated into top and bottom layers, denoted as $3SO_4$/0.5TFSI. The $3SO_4$/1.0TFSI was prepared by changing the $Zn(TFSI)_2$ concentrations using the same method. $Zn(TFSI)_2$ was introduced into deionized water to prepare a 0.5 m $Zn(TFSI)_2$ electrolyte. A baseline electrolyte (BE) was prepared by dissolving 43.13 g of $ZnSO_4 \cdot 7H_2O$ in deionized water in a 50 mL volumetric flask.

1.3. Preparation of PANI cathode

The PANI cathode material was prepared according to a previously reported procedure.[1] The commercial PANI was mixed with Ketjen Black and PVDF in a mass ratio of 7:2:1. The above mixture was homogeneously dispersed in NMP solvent. The slurry was coated on the graphite paper and dried at 120 ^oC for 10 h. The cathode material with 0.8-1.3 mg cm^{-2} active loading was achieved.

1.4. Material characterization

ICP-OES results were collected using an inductively coupled plasma-optical emission spectrometer (ICP-OES7200). Fourier transform infrared (FT-IR) spectra were recorded on a Nicolet iS50 spectrometer. An inVia Qontor spectrometer was used to record Raman spectra of electrolytes. ^1H nuclear magnetic resonance (^1H NMR) spectra were measured on an Avance

Neo 400 spectrometer. The crystalline structures of the samples were characterized by X-ray diffraction (XRD, DX-2700BH). The morphologies of Zn foils and elemental mapping were characterized by field-emission scanning electron microscopy (FESEM, Verios G4 UC) coupled with energy-dispersive X-ray spectroscopy (EDX). The contact angles of electrolytes on the Zn anode were tested using a contact angle tester. An elemental analyzer was applied to study the composition of the electrolytes. Ionic conductivity of electrolytes was measured using a DDS-307A conductivity meter. The viscosity of electrolytes was determined using a kinematic viscosimeter.

1.5. Electrochemical measurements

All Zn//Zn symmetric cells, Zn//Cu half cells, and Zn//PANI full batteries were assembled in CR2032 coin-type cells. In Zn//Cu half cells, Cu foil served as the working electrode, and Zn foil was used as the counter electrode and reference electrode. In Zn//Zn symmetric cells, two Zn foils were employed as electrodes, and 90 μL of electrolyte was applied for the electrochemical test. Cyclic voltammetry (CV), Tafel plots, Electrochemical impedance spectroscopy (EIS), chronoamperometry (CA), and linear sweep voltammetry (LSV) tests were performed on a CHI 760E electrochemical workstation. Additional electrochemical performance tests were conducted using a Land battery testing system. To verify the practicality of the BLE, the Zn//PANI full cells were assembled with a Zn foil as the anode and PANI as the cathode. A PP membrane and a glass fiber filter were utilized as separators for the biphasic system. First, the PANI cathode was placed at the bottom of the cell. The Zn foil, as the anode, was then positioned above it. Then the AE and OE were added, with each cell containing 60 μL of AE and 30 μL of OE as the BLE. Consequently, for the cells based on BLE, a hydrophilic glass fiber near the cathode was wetted by the AE, and the OE wetted a hydrophobic PP membrane near the anode. The cell was assembled by simply stacking the electrodes and the wetted separator layer by layer. The different hydrophiles of the separators facilitate the combination of two immiscible liquids into a robust biphasic system.

1.6. Theoretical Calculation

Classical density functional theory (DFT) calculations were performed for biphasic liquid electrolytes using the GROMACS 2020.6 software[2] to simulate the phase-separation process. The simulated electrolytes were constructed by randomly placing cations, Zn^{2+}, and water

molecules in a cubic box with proportional ratios using the Packmol software package.[3] Visualization of trajectories was realized using software VMD[4] and OVITO.[5] General Amber force field (GAFF) parameters were employed for MD to describe electrolytes studied in this work. NPT ensemble was performed for 30 ns to obtain the correct density of the electrolytes using the Berendsen barostat. The V-rescale temperature coupling method was applied to couple the temperatures. Afterward, a 40 ns production simulation was performed in the NVT ensemble for subsequent analysis. The binding energies of hydrogen-bonding, the Zn^{2+} solvation structure, and the electrostatic potential (ESP) mapping were assessed by the B3LYP functional of DFT calculations with 6-311++G** basis set method using the Gaussian16 program. The single conformation two-stage restraint electrostatic potentials (RESP) method developed by Bayly et al. was used to obtain the atomic charges by fitting the electrostatic potential calculated at the same level.[6] Self-diffusion coefficients of cations and anions were calculated consistently at 25 °C (298 K). The Vienna Ab Initio Package (VASP) was employed to perform all the density functional theory (DFT) calculations within the generalized gradient approximation (GGA) using the Perdew, Burke, and Ernzerhof (PBE) formulation. A plane wave basis set with a kinetic energy cutoff of 500 eV and a gamma-centered Monkhorst-Pack Grid. The adsorption energies (E_{ads}) are calculated as $E_{ads} = E_{ads/sub} - E_{ad} - E_{sub}$, where $E_{ad/sub}$, $E_{ad,}$ and E_{sub} are the optimized adsorbate/substrate system, the adsorbate in the structure, and the clean substrate, respectively.

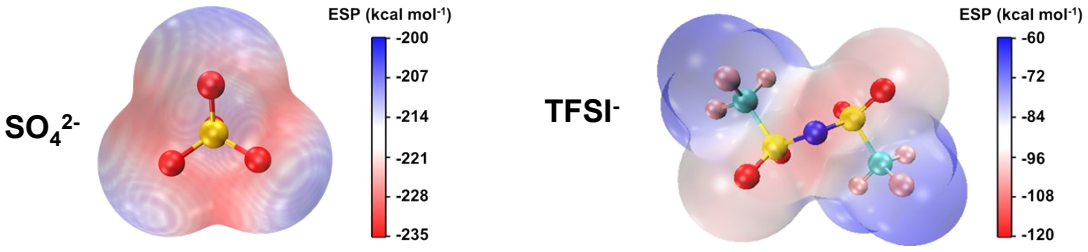

Fig. S1 Electrostatic potential mapping of SO_4^{2-} and $TFSI^-$.

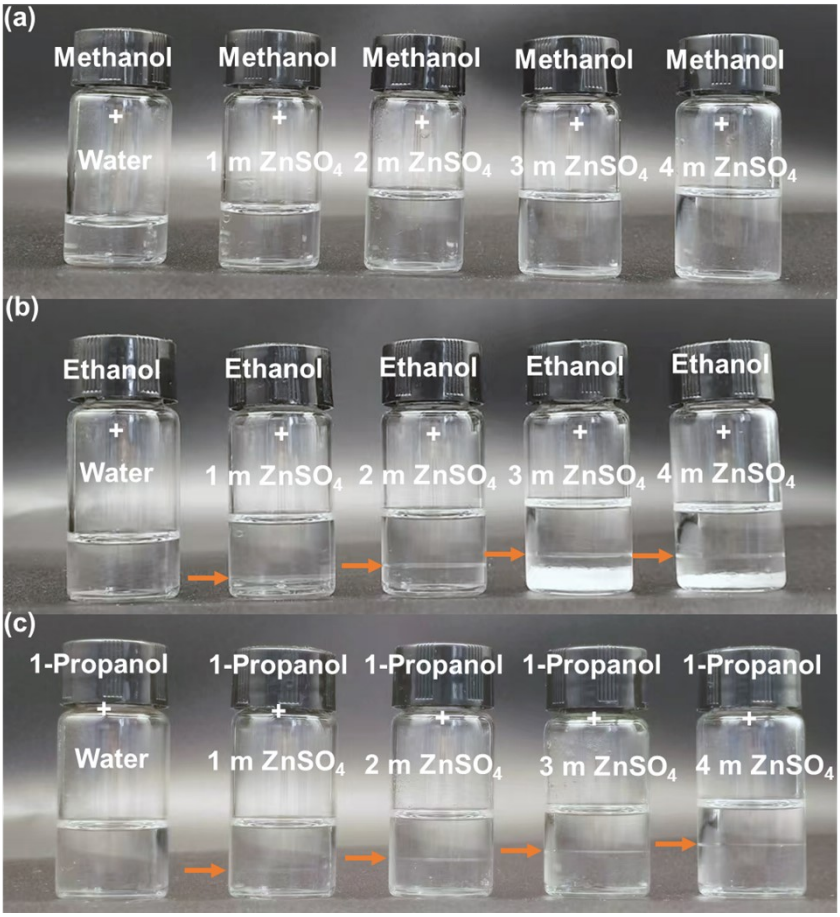

Fig. S2 Photographs of various organic solvent/water hybrid systems (1:1, v/v) with a certain amount of $ZnSO_4$.

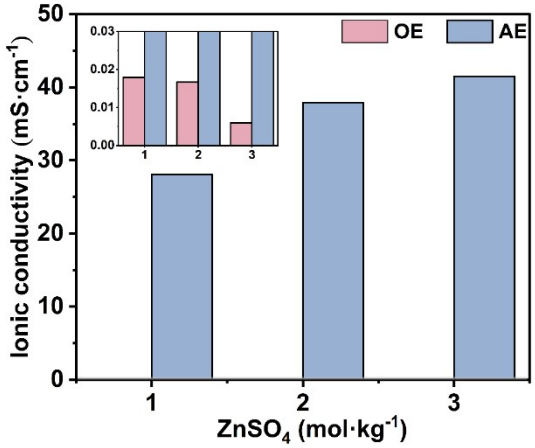

Fig. S3 Effect of different concentrations of $ZnSO_4$ on ionic conductivity of the biphasic system.

Fig. S4 Digital photos of biphasic liquid electrolytes with various $Zn(TFSI)_2$ concentrations.

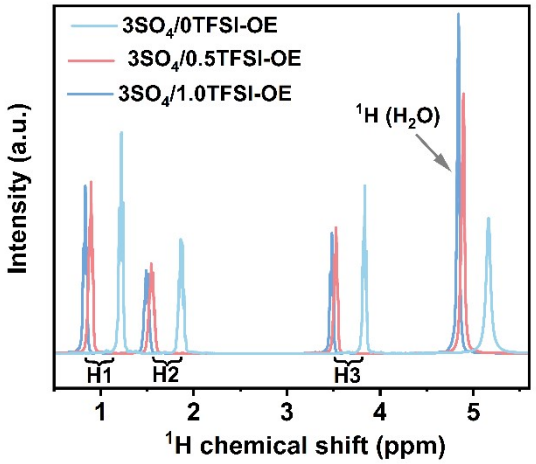

Fig. S5 ^1H NMR spectra for pure H_2O solution and the OE of different BLE.

The quantitative ^1H NMR analysis reveals a linear correlation between integral intensities and molar concentrations, as evidenced by the calibration curves in Figure S7. For the $3SO_4$/0TFSI system, 1-propanol and water molecules meet the following formula in the OE and AE phases:

$$n_{H2O\text{-}OE}=0.77n_{1\text{-}Propanol\text{-}OE} \quad (1)$$

$$n_{H2O\text{-}AE}=102.28n_{1\text{-}Propanol\text{-}AE} \quad (2)$$

For the $3SO_4$/0.5TFSI biphasic liquid electrolyte system, the stoichiometric ratios of 1-Propanol to water within the OE phase and AE phases exhibit precise phase-dependent partitioning:

$$n_{H2O\text{-}OE}=1.34n_{1\text{-}Propanol\text{-}OE} \quad (3)$$

$$n_{H2O\text{-}AE}=152.43n_{1\text{-}Propanol\text{-}AE} \quad (4)$$

For the $3SO_4$/1.0TFSI biphasic liquid electrolyte system：

$$n_{H2O\text{-}OE}=1.75n_{1\text{-}Propanol\text{-}OE} \quad (5)$$

$$n_{H2O\text{-}AE}=231.55n_{1\text{-}Propanol\text{-}AE} \quad (6)$$

n_{H2O-OE} and n_{H2O-AE} are the moles of H_2O in the OE and AE phases, respectively; $n_{1\text{-}Propanol-OE}$ and $n_{1\text{-}Propanol\text{-}AE}$ are the moles of 1-propanol in the OE and AE phases, respectively. In all the

above biphasic liquid electrolyte systems, the total mass of H_2O is 1 g. The total mass of 1-propanol in the electrolyte system is 0.8 g. These lead to the following relationship:

$$n_{H2O\text{-}OE}+n_{H2O\text{-}AE}=0.0556\text{mol} \quad (7)$$

$$n_{1\text{-}Propanol-OE}+n_{1\text{-}Propanol\text{-}AE}=0.0133\text{mol} \quad (8)$$

Combined equations (7) to (8), for the $3SO_4$/0TFSI biphasic liquid electrolyte system, we can obtain that:

$$n_{1\text{-}Propanol\text{-}OE}=12.90\ \text{mmol}$$

$$n_{1\text{-}Propanol\text{-}AE}=0.40\ \text{mmol}$$

$$n_{H2O\text{-}OE}=9.93\ \text{mmol}$$

$$n_{H2O\text{-}AE}=45.67\ \text{mmol}$$

Therefore, the mass of the solvent in the OE and AE phases can be obtained.

$$m_{1\text{-}Propanol\text{-}OE}=0.77\ \text{g}$$

$$m_{1\text{-}Propanol\text{-}AE}=0.02\ \text{g}$$

$$m_{H2O\text{-}OE}=0.18\ \text{g}$$

$$m_{H2O\text{-}AE}=0.82\ \text{g}$$

Similarly, for the $3SO_4$/0.5TFSI biphasic liquid electrolyte system, the mass of solvent in the OE and AE phases can be obtained.

$$m_{1\text{-}Propanol\text{-}OE}=0.78\ \text{g}$$

$$m_{1\text{-}Propanol\text{-}AE}=0.22\ \text{g}$$

$$m_{H2O\text{-}OE}=0.31\ \text{g}$$

$$m_{H2O\text{-}AE}=0.69\ \text{g}$$

For the $3SO_4$/1.0TFSI biphasic electrolyte system:

$$m_{1\text{-}Propanol\text{-}OE}=0.79\ \text{g}$$

$$m_{1\text{-}Propanol\text{-}AE}=0.01\ \text{g}$$

$$m_{H2O\text{-}OE}=0.42\ \text{g}$$

$$m_{H2O\text{-}AE}=0.58\ \text{g}$$

In summary, for all the aforementioned biphasic liquid electrolyte systems, the OE phase consistently exhibits enrichment in 1-propanol, whereas the AE phase is characterized by aqueous dominance. For example, in the $3SO_4$/0TFSI biphasic liquid electrolyte·system, the OE phase comprises 81.20 wt.% 1-propanol and 18.8 wt.% H_2O, with the AE phase containing 96.50 wt.% H_2O and 3.50 wt.% 1-propanol.

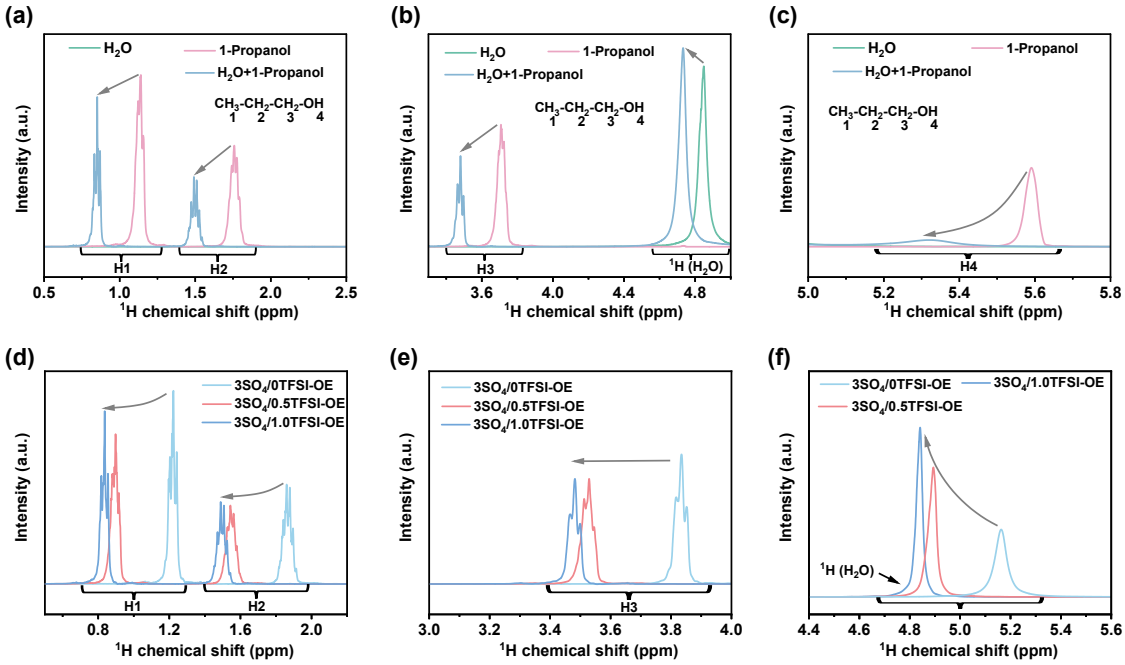

Fig. S6 ^{1}H NMR spectra for pure water, 1-propanol, water/1-propanol hybrid system, and the OE of different BLE.

The ^{1}H resonances from $-CH_3$, $-CH_2-CH_3$, and $-CH_2-$ of pure 1-propanol are at 1.14 ppm, 1.76 ppm, and 3.71 ppm, respectively. The ^{1}H peak of pure water is at 4.84 ppm. The protons of 1-propanol and H_2O shift upfield after the introduction of 1-propanol, indicating there is higher electron density around the H atoms, which means more electron shielding. The hydrogen-bonding (HB) interaction between the O atom in 1-propanol and the H atom in H_2O can be attributed to this result. Compared to the pure $3SO_4$/0TFSI-OE, the protons of 1-propanol and H_2O continuously shift upfield with the increasing concentration of $Zn(TFSI)_2$. These results reveal that the chaotropic $TFSI^-$ can interact with water to reform HBs, during which the HBs in water were largely destroyed.

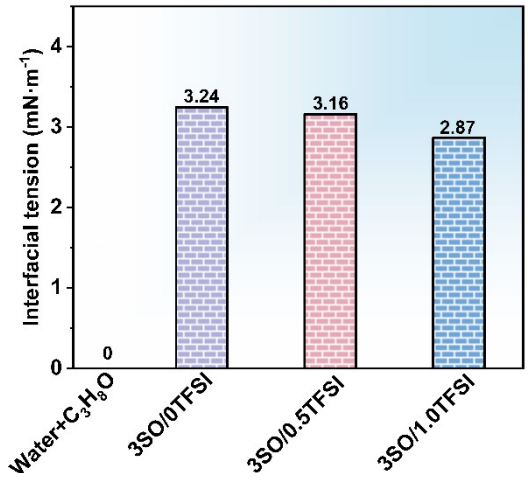

Fig. S7 Interfacial tension of BLE systems.

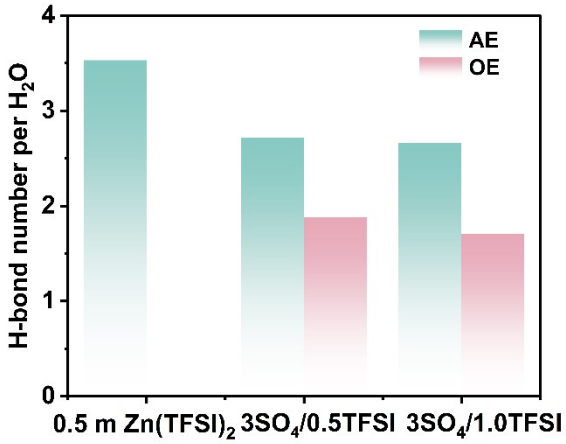

Fig. S8 The average HB number formed per H_2O molecule in different electrolytes obtained from simulations.

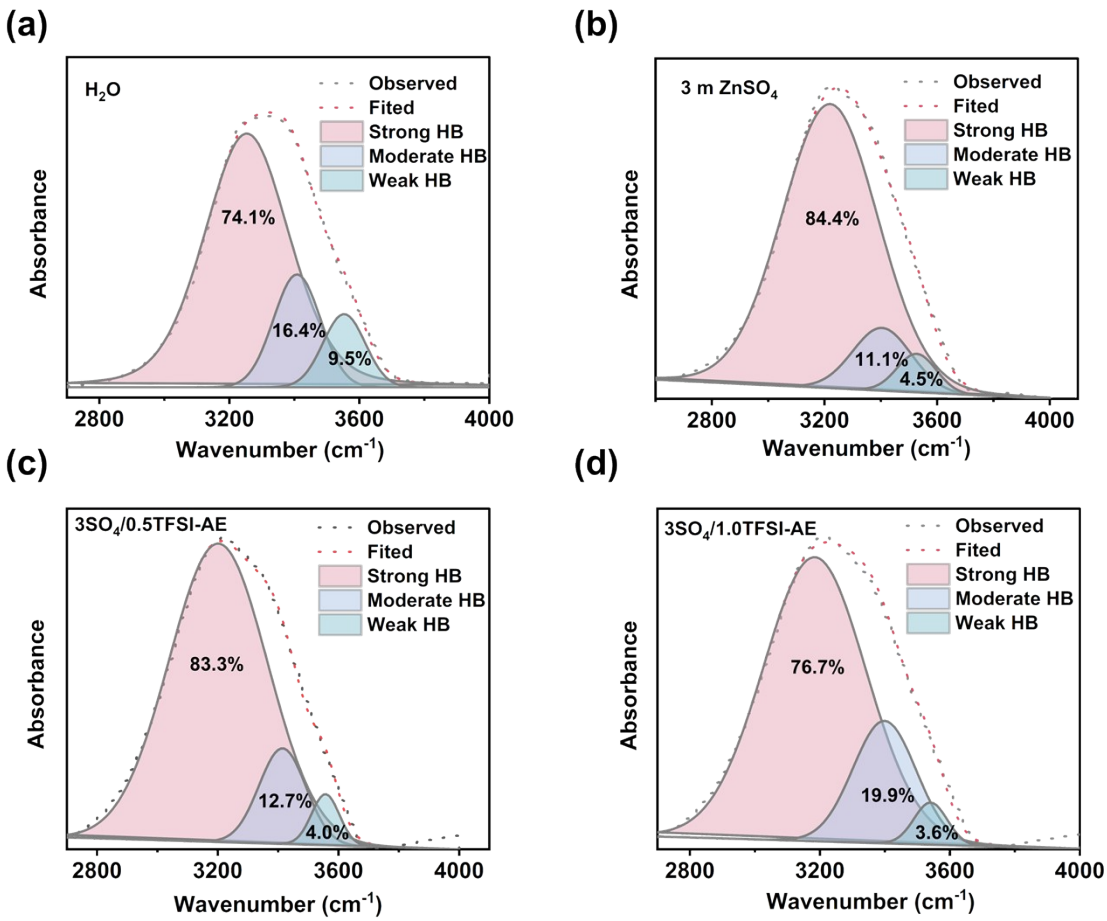

Fig. S9 FT-IR spectra of the AE with different BLE systems.

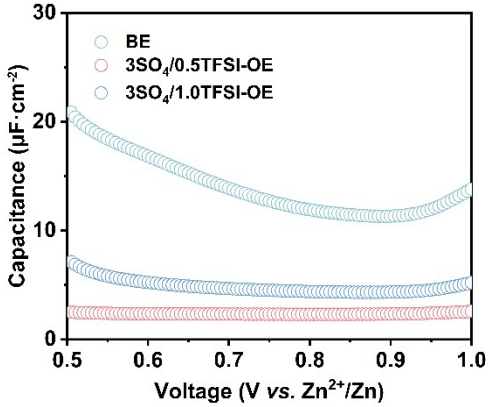

Fig. S10 Differential capacitance curves are conducted in different electrolytes.

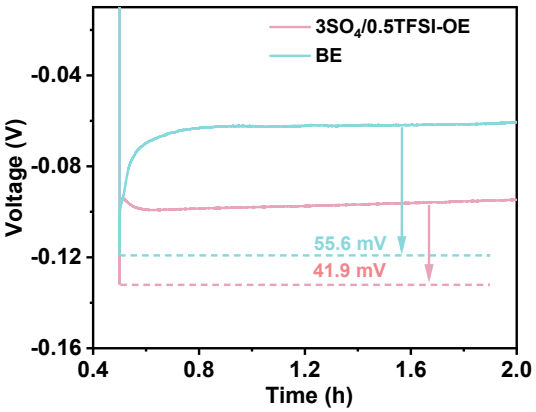

Fig. S11 Nucleation overpotential based on the Zn substrate in different electrolytes at a current density of 1.0 mA·cm^{-2}.

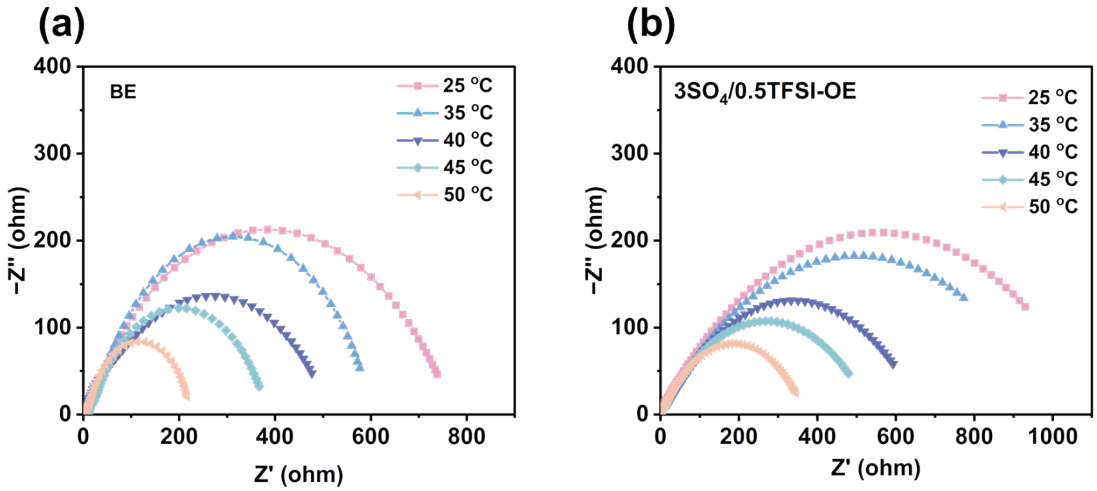

Fig. S12 Nyquist plots at different temperatures in the (a) BE and (b) $3SO_4$/0.5TFSI-OE.

To further investigate the interfacial charge transfer process, the temperature-dependent impedance measurements were carried out at elevated temperatures between 25 and 50 °C. The plots of $\ln(R_{ct}^{-1})$ versus reciprocal temperature were fitted by the Arrhenius equation:

$$1/R_{ct}^{-1}=A_0\exp(-E_a/RT)$$

where R_{ct}, A_0, R, and T represent the charge-transfer resistance at different temperatures, frequency factor, ideal gas constant, and absolute temperature, respectively.

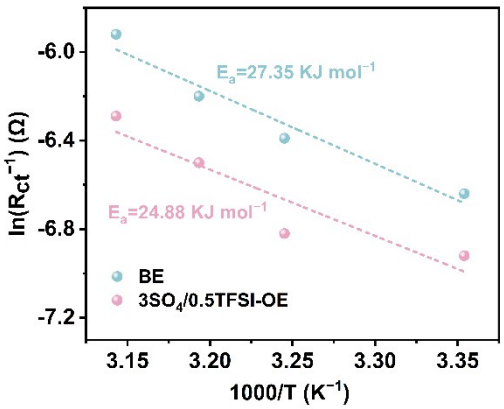

Fig. S13 Arrhenius curves in the BE and $3SO_4$/0.5TFSI-OE.

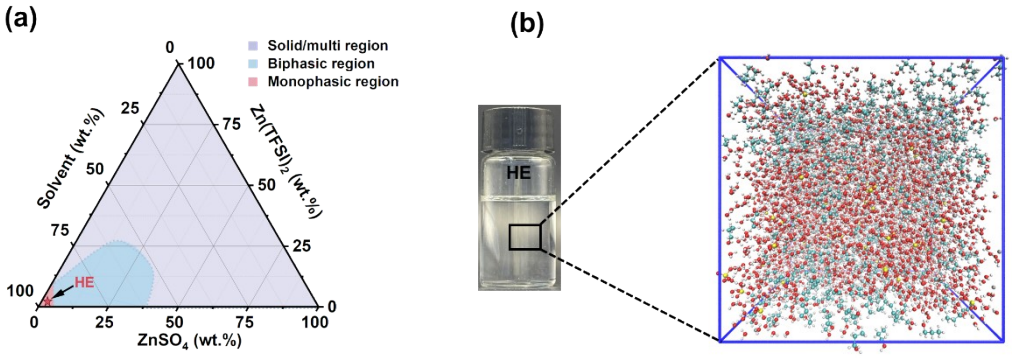

Fig. S14 Ternary phase diagram of solvent/$Zn(TFSI)_2$/$ZnSO_4$ mixtures at 25 °C; (b) Snapshot of the MD simulation and schematic structure of the HE.

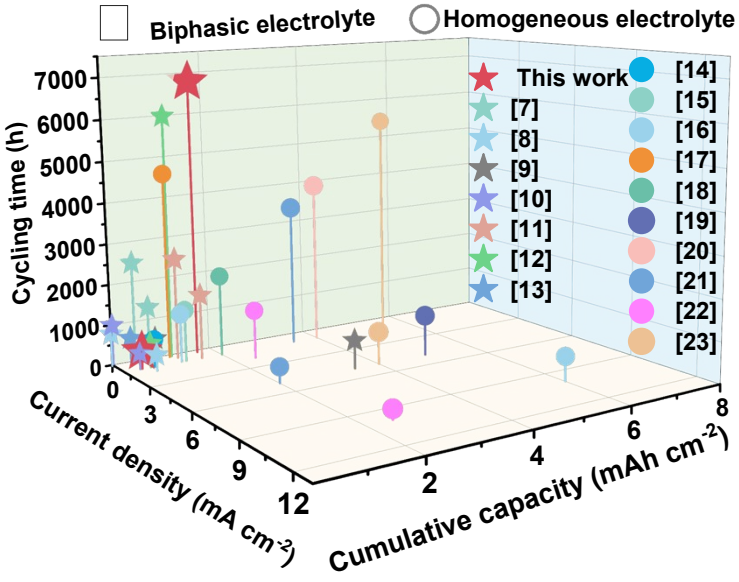

Fig. S15 Comparison of cycling stability with recently reported electrolyte results at different current densities and capacities.

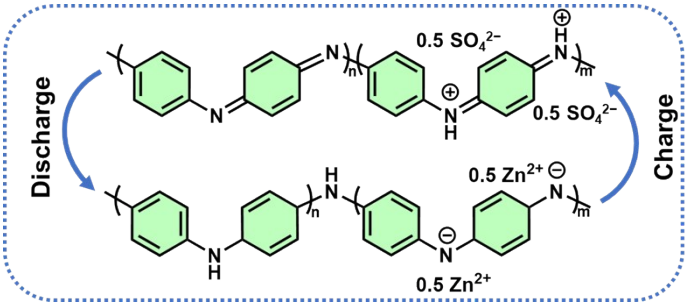

Fig. S16 Redox processes of the PANI cathode.

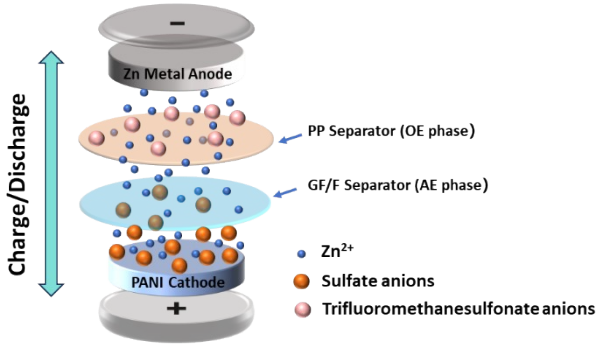

Fig. S17 Schematic diagram of the structure of Zn//PANI cell.

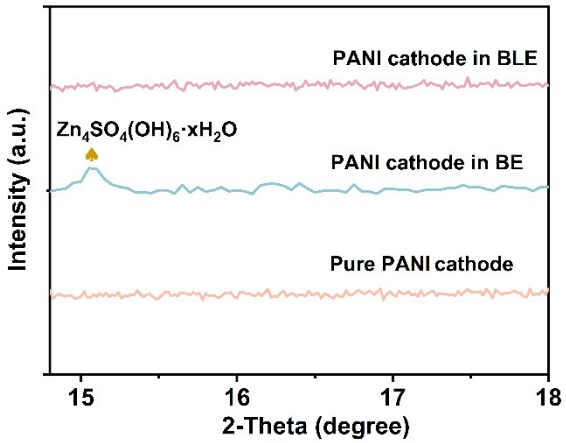

Fig. S18 XRD patterns of pure PANI cathode and PANI cathode in BE after the 500 th cycle and BLE after the 800 th cycle at a current density of 0.1 A g^{-1}.

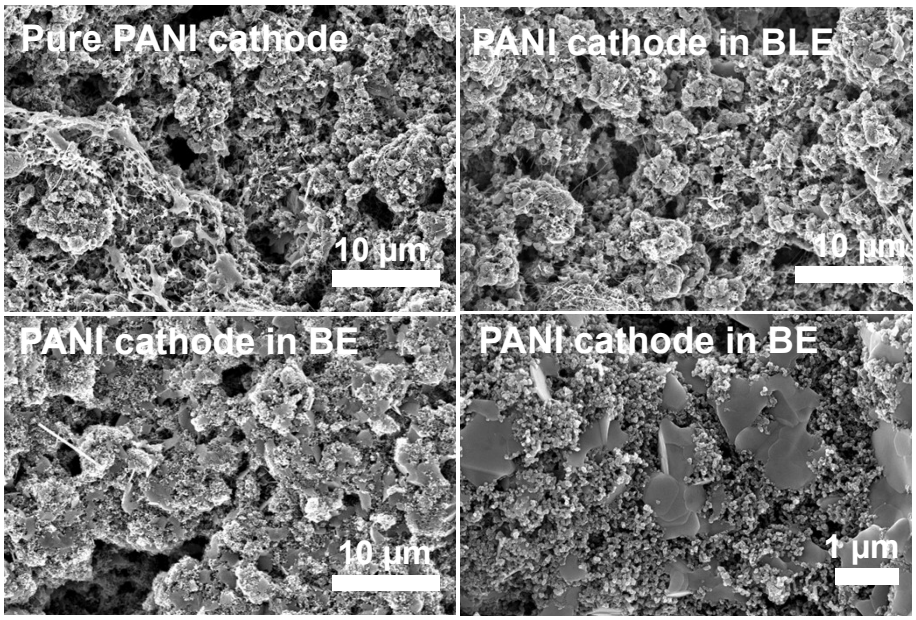

Fig. S19 SEM images of pure PANI cathode, PANI cathode in BE after 500 th cycle, and PANI cathode in BLE after 800 th cycle at a current density of 0.1 A g^{-1}.

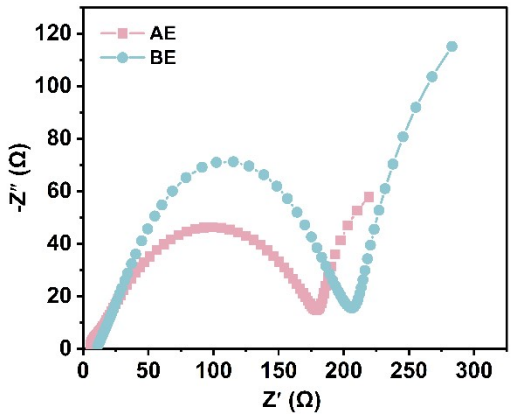

Fig. S20 EIS curves of Zn//PANI full cells in BE and AE.

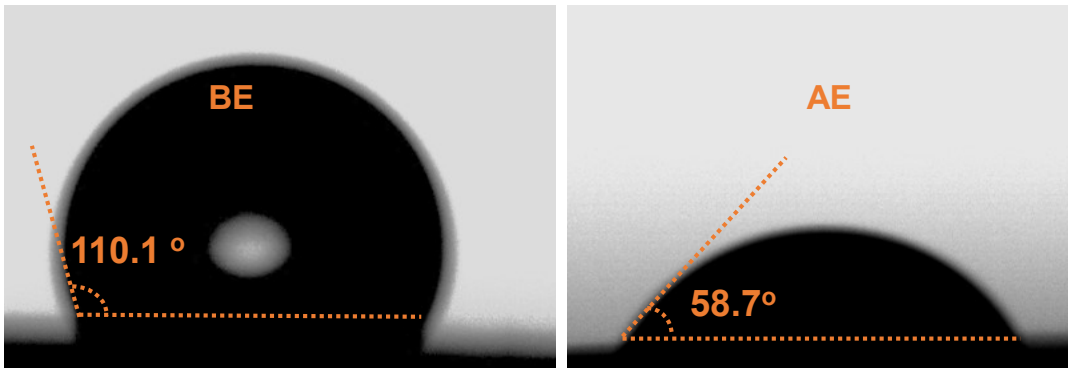

Fig. S21 Contact angle of the BE and AE on the PANI cathode.

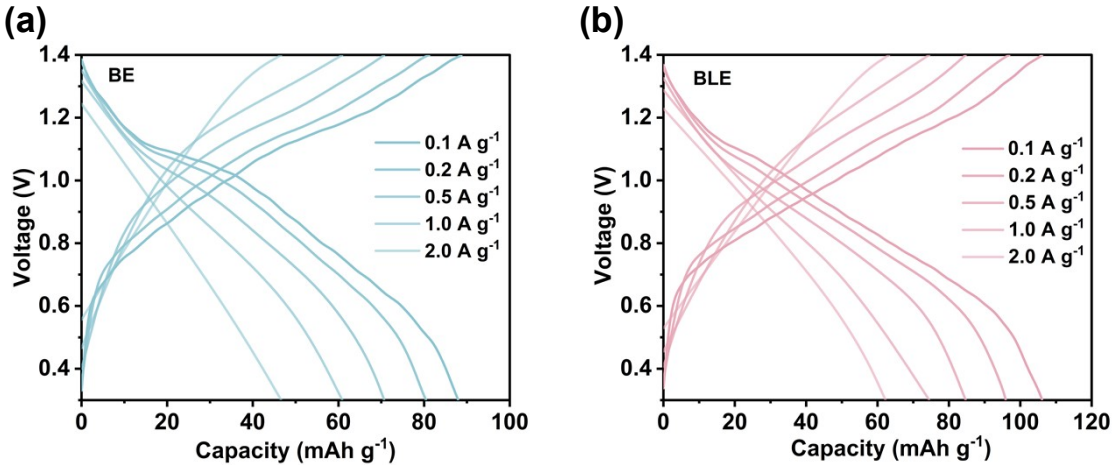

Fig. S22 Galvanostatic charge/discharge profiles of Zn//PANI full cells using BE and (b) BLE at different current densities.

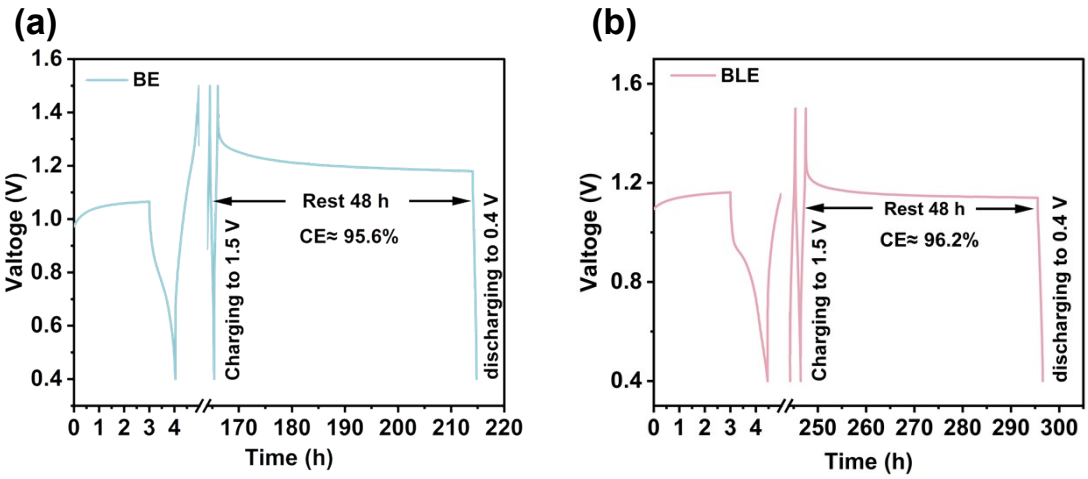

Fig. S23 (a) Storage performance of the Zn//PANI cells in the BE and (b) BLE.

Table S1. The density results of different electrolytes.

Sample	$3SO_4$/0TFSI	$3SO_4$/0.5TFSI	$3SO_4$/1.0TFSI
OE	0.86	0.92	1.06
AE	1.38	1.42	1.45

Table S2. The results of the concentration distribution of different elements in the OE obtained by ICP-OES.

Sample	m/mg	C/%	N/%	H/%	S/%
$3SO_4$/0.5TFSI-OE	2.18	6.46	3.82	1.58	17.85
$3SO_4$/1.0TFSI-OE	2.47	0.19	3.87	1.63	18.03

Table S3. The results of the concentration distribution of different elements in the AE obtained by ICP-OES.

Sample	m/mg	C/%	N/%	H/%	S/%
$3SO_4$/0.5TFSI−AE	1.90	0.19	0.13	1.10	17.33
$3SO_4$/1.0TFSI−AE	2.00	0.56	0.34	1.10	17.53

Table S4. Comparison of electrochemical performance with recently reported results.

Electrolyte	Current density (mA cm^{-2})	Cycling time (h)	Cumulative capacity (Ah cm^{-2})	Reference
1 M $Zn(TFSI)_2$+0.5 M $MgSO_4$-FDMA/1.0 M $ZnSO_4$-H_2O	0.2 0.5	2500 1400	0.5 0.7	[7]
0.5 M $Zn(TFSI)_2$-AN/3.4 M $ZnSO_4$	1.5 0.1	400 800	0.6 0.08	[8]
0.9 M $Zn(TFSI)_2$-NMP/1 M $ZnSO_4$	5 1	700 700	3.5 0.7	[9]
1.15 M $ZnSO_4$-PEG-200-H_2O	1 0.1	400 1012	0.4 0.1012	[10]
1 M $Zn(PES)_2$-H_2O	1 0.25 0.5	1600 1750 1250	1.6 1.75 1.25	[11]
4 M $Zn(OTF)_2$-TEP-H_2O	0.2 1.0	1200 600	1.2 0.6	[12]
1.0 M $Zn(TFSI)_2$-TFEP-H_2O	0.5	700	0.35	[13]
0.5 M $Zn(TFSI)_2$-1-Propanol/3 M $ZnSO_4$	1 0.25	440 6800	0.44 1.7	This work

References

1 H. Du, X. Qi, L. Qie, Y. Huang, *Adv. Funct. Mater.* 2023, **33**, 2302546.

2 M. J. Abraham, T. Murtola, R. Schulz, S. Páll, J. C. Smith, B. Hess, E. Lindahl, *Software X* 2015, **1-2**, 19-25.

3 L. Martínez, R. Andrade, E. G. Birgin, J. M. Martínez, *J. Comput. Chem.* 2009, **30**, 2157-2164.

4 W. Humphrey, A. Dalke, K. Schulten, *J. Mol. Graph.* 1996, **14**, 33-38.

5 A. Stukowski, *Model. Simul. Mater. Sci. Eng.* 2010, **18**, 015012.

6 C. I. Bayly, P. Cieplak, W. Cornell, P. A. Kollman, *J. Phys. Chem.* 1993, **97**, 10269-10280.

7 X. Zhao, J. Fu, M. Chen, Y. Wang, C. Huang, K. Qian, G. Feng, B. Li, D. Zhou, F. Kang, *J. Am. Chem. Soc.* 2025, **147**, 2714-2725.

8 W.-Y. Kim, H.-I. Kim, K. M. Lee, E. Shin, X. Liu, H. Moon, H. Adenusi, S. Passerini, S. K. Kwak, S.-Y. Lee, *Energy Environ. Sci.* 2022, **15**, 5217-5228.

9 H. Fan, H. Zhang, Q. Liu, M. Li, L. Liu, J. Gao, Q. Zhang, E. Wang, *ACS Energy Lett.* 2023, **8**, 4338-4348.

10 J. Zhou, B. Hao, H. Yang, H. Ao, T. Qian, Z. Wang, C. Yan, *Nano Lett.* 2025, **25**, 4809-4817.

11 Y. Zhao, M. Ouyang, Y. Wang, R. Qin, H. Zhang, W. Pan, D. Y. C. Leung, B. Wu, X. Liu, N. P. Brandon, J. Xuan, F. Pan, H. Wang, *Adv. Funct. Mater.* 2022, **32**, 2203019.

12 J. Zhu, M. Yang, Y. Hu, M. Yao, J. Chen, Z. Niu, *Adv. Mater.* 2024, **36**, 2304426.

13 L. Cao, D. Li, T. Deng, Q. Li, C. Wang, *Angew. Chem. Int. Ed.* 2020, **59**, 19292-19296.

14 L. Yu, J. Huang, S. Wang, L. Qi, S. Wang, and C. Chen, *Adv. Mater.* 2023, **35**, 2210789.

15 D. G. Vazquez, T. P. Pollard, J. Mars, J. M. Yoo, H.-G. Steinrück, S. E. Bone, O. V. Safonova, M. F. Toney, O. Borodin, M. R. Lukatskaya, *Energy Environ. Sci.* 2023, **16**, 1982-1991.

16 H. Qin, W. Kuang, N. Hu, X. Zhong, D. Huang, F. Shen, Z. Wei, Y. Huang, J. Xu, H. He, *Adv. Funct. Mater.* 2022, **32**, 2206695.

17 Y. Chen, S. Zhou, J. Li, X. Zhang, C. Zhou, X. Shi, C. Zhang, G. Fang, S. Liang, Z. Su, A. Pan, *Angew. Chem. Int. Ed.* 2025, **64**, e202423252.

18 S. Chen, D. Ji, Q. Chen, J. Ma, S. Hou, and J. Zhang, *Nat. Commun.* 2023, **14**: 3526

19 M. Xu, F. Liu, L. Chen, Y. Lei, Z. Liu, T. Abdiryim, F. Xu, J. You, Y. Tan, Z. Tan, X. Liu. *Energy Stor. Mater.* 2025, **80**, 104373.

20 L. Chang, S. Bi, J. Li, Q. Sun, X. Lu, and H. Cheng, *ACS Nano* 2025, **19**, 27424−27439.

21 Y. Lv, M. Zhao, Y. Du, Y. Kang, Y. Xiao, and S. Chen, *Energy Environ. Sci.* 2022, **15**, 4748-4760.

22 Y. Chu, S. Zhang, S. Wu, Z. Hu, G. Cui, and J. Luo, *Energy Environ. Sci.* 2021,**14**, 3609-3620.

23 X. Chen, C. Liu, X. Bai, J. Zhang, X. Chang, L. Hou, H. Huang, Y. Wei, B. Wu, W. Liu, Q. Wang, *Energy Stor. Mater.* 2025, **75**, 103984.